



HAL
open science

Relation between Surface Composition and Electronic Properties of Native Oxide Films on an Aluminium-Copper Alloy Studied by DFT

P. Cornette, Dominique Costa, P. Marcus

► **To cite this version:**

P. Cornette, Dominique Costa, P. Marcus. Relation between Surface Composition and Electronic Properties of Native Oxide Films on an Aluminium-Copper Alloy Studied by DFT. *Journal of The Electrochemical Society*, 2020, 167 (16), pp.161501. 10.1149/1945-7111/abc9a1 . hal-03095024

HAL Id: hal-03095024

<https://hal.science/hal-03095024>

Submitted on 5 Jan 2021

HAL is a multi-disciplinary open access archive for the deposit and dissemination of scientific research documents, whether they are published or not. The documents may come from teaching and research institutions in France or abroad, or from public or private research centers.

L'archive ouverte pluridisciplinaire **HAL**, est destinée au dépôt et à la diffusion de documents scientifiques de niveau recherche, publiés ou non, émanant des établissements d'enseignement et de recherche français ou étrangers, des laboratoires publics ou privés.

OPEN ACCESS

Relation between Surface Composition and Electronic Properties of Native Oxide Films on an Aluminium-Copper Alloy Studied by DFT

To cite this article: P. Cornette *et al* 2020 *J. Electrochem. Soc.* **167** 161501

View the [article online](#) for updates and enhancements.

239th ECS Meeting

with the 18th International Meeting on Chemical Sensors (IMCS)

ABSTRACT DEADLINE: DECEMBER 4, 2020





May 30-June 3, 2021

SUBMIT NOW →



Relation between Surface Composition and Electronic Properties of Native Oxide Films on an Aluminium-Copper Alloy Studied by DFT

P. Cornette, D. Costa,^z  and P. Marcus^{*} 

Chimie ParisTech, PSL University, CNRS, Institut de Recherche de Chimie Paris, Physical Chemistry of Surfaces Research Group, 75005 Paris, France

We performed a DFT modelling of $\text{Al}_2\text{O}_3(001)/\text{Al}(001)$ and $\text{Al}_2\text{O}_3(001)/\text{Al}_2\text{Cu}(001)$ surfaces and of $\text{Al}(010)/\text{Al}_2\text{Cu}(010)$ interfaces covered with $\text{Al}_2\text{O}_3(001)$. We focus on the electronic properties (work function, valence band and electronic gap) computed for the different models. We show that both on Al and Al_2Cu , the oxide layer induces a significant increase in work function. The effect of the composition of the first metallic layer underneath the oxide film is also investigated. Cu enrichment under the oxide film induces an increase in work function, however less marked than the one caused by the oxide layer. We show that the work function increase is due to a charge transfer from the interfacial metal layer to the oxide layer. The same result is found at the oxidized $\text{Al}(010)/\text{Al}_2\text{Cu}(010)$ interface. The work function of the oxidized Al_2Cu zone is higher than the one of oxidized Al.

© 2020 The Author(s). Published on behalf of The Electrochemical Society by IOP Publishing Limited. This is an open access article distributed under the terms of the Creative Commons Attribution 4.0 License (CC BY, <http://creativecommons.org/licenses/by/4.0/>), which permits unrestricted reuse of the work in any medium, provided the original work is properly cited. [DOI: 10.1149/1945-7111/abc9a1]



Manuscript submitted September 22, 2020; revised manuscript received November 10, 2020. Published November 24, 2020. *This paper is part of the JES Focus Issue on Characterization of Corrosion Processes in Honor of Philippe Marcus.*

Supplementary material for this article is available [online](#)

DFT calculations are increasingly used to better understand the corrosion resistance properties of metals and alloys. Papers now often combine experimental works with DFT calculations. In particular, in the case of Al alloys and/or intermetallic particles (IMPs), several joint experimental and theoretical works have been performed, where theory helps in interpreting the experimental data.^{1–9} In other works, DFT models are used to represent typical corrosion situations e.g. alloy dissolution.^{1,10} The adsorption of corrosive ions (such as chlorides) was also undertaken with DFT studies.^{11–15} Some theoretical papers focused on work function calculation and comparison between different Al and Al_2Cu surfaces, in order to better understand the effect of surface composition and termination on the work function value.^{2,16,17} The work function is the minimum energy needed to emit an electron from the surface to vacuum, implying that a higher work function corresponds to a higher resistance against losing electrons, and vice versa. The work function is an appropriate measure of the electronegativity^{18,19} and the work function value indeed leads to a reasonable estimated trend of charge transfer for molecular adsorbates.¹⁸ The work function is also one possible descriptor of metal nobility, as recently reviewed.²⁰ As work function values are easy to extract from DFT calculations, theoretical works have correlated their values with the nobility of the metals/alloys.^{1–3,12,21} The calculated work function can be compared to the experimentally measured Volta potential in dry conditions. In vacuum, the work function, Φ , is simply correlated to the Volta potential Ψ , with $e\Psi = \Phi$. The presence of solvent renders the things more intricate.²² Nevertheless, the Volta potential has been considered as an indicator for the corrosion tendency,²³ and this was applied to the study of IMPs by Frankel et al. who found a linear relation between the Volta potential measured in air and the corrosion potential in aqueous solution for a range of pure metal and alloys.^{24,25} Leygraf et al.^{17,21} combined Scanning Kelvin Probe Force Microscopy (SKPFM) measurements of Volta potential on Al alloys and IMPs, with DFT calculations of work function. The computational results of Volta potential differences between the IMPs and the surrounding aluminium matrix were compared to SKPFM measurements.^{2,17,21} The first principles calculations were performed on models of Al and Al_2Cu surfaces. Various crystal

faces and terminations of Al_2Cu were examined, showing that both the nature of the face and its termination have a significant effect on the work function value, which varies between 4.0 and 4.5 eV for Al_2Cu (to be compared to the value of 4 eV for Al). The authors reported the averaged calculated Volta potential difference, $\Delta\Psi$, between Al_2Cu surfaces and pure Al to be +109 mV, confirming the more noble character provided by copper. However, this value is much lower than the experimental values ($\Delta\Psi =$ between +550 and 700 mV). To explain this difference, the authors invoked the presence of an adsorbed oxygen and hydroxyl-containing species or a thin oxide and hydroxide film, which can significantly increase the Volta potential. In a further study,²¹ the authors consider the Al_2Cu surface terminations in adding water molecules above the surfaces. They observed a significant effect of the presence of adsorbed water on the calculated work function of Al_2Cu , which varied between 3.2 and 4.5 eV. Interestingly, whereas the dry surfaces have a higher Φ than Al, (4.3–4.5 eV vs 4.16 for Al), the reverse was observed in the presence of 2 water layers, with the Al work function unchanged, but Al_2Cu Φ decreased by 0.25–0.45 eV, suggesting that depending on the surface termination and water loading, the intermetallic particle potential might be anodic or cathodic vs the Al matrix.

In a recent paper by Li et al.,⁷ the passive films on Al and Al_2CuMg were analysed. AES data show that the passive layer on Al is thicker than on Al_2CuMg . The authors modelled with DFT several surfaces, namely Al(100), Al(111), Al(101), $\text{Al}_2\text{CuMg}(101)$ and $\text{Al}_2\text{CuMg}(001)$. According to the density functional theory (DFT) calculations, the average charge transfers and adsorption energies of the adsorbates ($\text{O}_2/\text{OH}/\text{H}_2\text{O}$) on the Al surfaces are larger than those on the Al_2CuMg surfaces, meaning that O_2 and H_2O preferably dissociate and adsorb on the Al surfaces. Moreover, the electronic interactions between the adsorbates and Al surfaces are stronger. The authors conclude that this is the reason why the growth rate of the passive film on the Al_2CuMg particle is slower. Adsorption of water and Cl on Al_2Cu (001) surface was investigated.²⁶ It was found that Al surface sites are more energetically favorable for Cl^- ions and water than copper sites. Finally, we mention that some recent theoretical papers have studied the semi-coherent Al// Al_2Cu interface: the (001)Al//(001) Al_2Cu , (010)Al//(010) Al_2Cu ,²⁷ (110) Al_2Cu /(111)Al,²⁸ (001) Al_2Cu /(001)Al, (010) Al_2Cu /(010)Al interface,²⁹ (001) Al_2Cu /{001}Al and [0 1 0] Al_2Cu /[0 1 0]Al³⁰ interfaces have been modelled.

*Electrochemical Society Fellow.

^zE-mail: dominique.costa@chimieparitech.psl.eu

All these studies, albeit giving interesting qualitative information, did not consider a real oxide covering the $\text{Al}_2\text{Cu}(\text{Mg})$ and Al surfaces. To the best of our knowledge, no oxidized Al_2Cu surfaces have yet been modelled. Models of oxidized metals are not easy to build, and in fact there is, to our knowledge, a limited number of models of Al-supported aluminium oxides.^{6,31,32} Gronbeck³² used $\alpha\text{-Al}_2\text{O}_3(0001)$ surface on Al(111), and showed that with increasing thickness, the surface reactivity in redox reactions decreases. The limiting thickness was found to be 18 Å. Lanthony et al.³¹ studied the first steps of Al(111) oxidation and provided a model containing two $\gamma\text{-Al}_2\text{O}_3$ like layers. We published a model of epitaxial supported $\gamma\text{-Al}_2\text{O}_3(111)$ on the Al(111) surface,⁶ and we varied the thickness of the oxide layer, from 5 to 12 Å. As in Ref. 32, we showed that increasing the thickness induces a decrease of the surface reactivity, the oxide layer being more protective against the cathodic reaction for thicknesses of 9 and 12 Å. We could directly explain the loss of reactivity towards dioxygen by an increase in the work function. We also showed that Cu monolayer segregation underneath the oxide film at low concentration tends to increase the work function, whereas a decrease of the work function by 0.3 eV is calculated at high concentration.³ Moreover, we used both Lanthony's model³¹ and our own model in theoretical works in which the adsorption of several organic molecules was studied, and the results compare well with experimental data.^{wang}

In a recent work,³³ we have analysed in details the native film formed on Al matrix and IMP particles on a model Al–Cu alloy. We reported the presence of chemical heterogeneities at the surface of the Al–Cu alloys. The surface is covered with an Al_2O_3 layer, but changes occur underneath this layer and several situations can be distinguished: Al covered with Al_2O_3 (Al/ Al_2O_3), Al with Cu segregated at the metal/oxide interface and covered with Al_2O_3 (Al–Cu_{seg}/ Al_2O_3), $\text{Al}_2\text{Cu}/\text{Al}$ terminated, covered with Al_2O_3 ($\text{Al}_2\text{Cu}\text{-Al}_{\text{term}}/\text{Al}_2\text{O}_3$), and $\text{Al}_2\text{Cu}\text{-Cu}$ terminated, covered with Al_2O_3 ($\text{Al}_2\text{Cu}\text{-Cu}_{\text{term}}/\text{Al}_2\text{O}_3$). The complexity of the systems makes difficult the prediction of the respective surface nobilities and related galvanic corrosion trend. To better understand the role of each identified parameter, oxide thickness, Cu enrichment, nature of the phase, we decided to build models which account for the surface heterogeneities observed experimentally. In the present work, we build models of oxidized Al and Al_2Cu surfaces, where the oxide layer is identical. This allows us i) to compare Al and Al_2Cu covered by an identical oxide, as is the case observed experimentally, ii) to study independently the influence of the metal composition on the electronic properties of the alloy/ Al_2Cu . We first describe briefly the model construction (more details being reported in the SI-1 section is available online at stacks.iop.org/JES/167/161501/mmedia). We analyse separately the Al and Al_2Cu surfaces covered with an oxide layer. In addition, we studied the influence of the interface metal/oxide layer composition. The outermost metal layer (and the metal/oxide interface) was substituted by metal atoms of increasing work function. This strategy allowed us to i) rationalize the link between work function of the metal and oxidized surfaces, ii) model surface segregation and enrichment under the oxide film, as observed experimentally.³³ We also report results on a oxidized Al(010)// Al_2Cu (010) commensurate interface. In a third part, we compare our results with previous works and with experimental data. Note that although the presence of Cu_2O islands was observed experimentally,³³ it will not be considered here.

Calculation Details

All calculations were performed using the periodic density functional theory (DFT) method based on the generalized gradient approximation (GGA),³⁴ employing the Perdew, Burke and Ernzerhof (PBE)³⁵ exchange-correlation functional as implemented in the plane-wave program Vienna ab initio simulation package (VASP).³⁶ The projector-augmented wave (PAW) potentials^{37,38} were used for the core electron representation with a PAW core radius of 1.52 Å for oxygen.

For the bulk materials, the simulation supercells contained 4 atoms for Al and Cu, 6 atoms for $\theta\text{-Al}_2\text{Cu}$ and 40 atoms for $\gamma\text{-Al}_2\text{O}_3$. The model of $\gamma\text{-Al}_2\text{O}_3$ was taken from the studies of Digne et al.³⁹ A converged K-points mesh of $(6 \times 6 \times 6)$ was used for bulk Al, Cu and $\theta\text{-Al}_2\text{Cu}$ and $(4 \times 4 \times 4)$ for Al_2O_3 . Within this approach, the bulk lattice constants are $a = 4.05$ Å for Al, $a = 3.63$ Å for Cu, $a = 5.98$ Å and $c = 4.74$ Å for $\theta\text{-Al}_2\text{Cu}$ and $a = 8.03$ Å, $b = 8.34$ Å and $c = 5.55$ Å for $\gamma\text{-Al}_2\text{O}_3$, in good agreement with experimental values and previous studies.^{6,40}

For each calculation, the quality of the basis set is determined by a single parameter, the energy cutoff (E_{cut}). In this work, we used $E_{\text{cut}} = 520$ eV and a smearing $\sigma = 0.01$ eV was applied. A dipolar correction was applied along the z axis. The integration in reciprocal space was performed with a Monkhorst-Pack⁴¹ grid $(3 \times 3 \times 1)$. Geometry optimizations performed all along this work were considered converged when the energy differences were inferior to 10^{-4} eV per cell.

Binding energies between metal and oxide are calculated as $E_b = E_{\text{met/ox}} - E_{\text{met}} - E_{\text{ox}}$, where E_{met} and E_{ox} are the energies of metal and oxide in the same geometry as when the interface is formed.

The work function was obtained by analysing the LOCPOT file provided in VASP, and reporting the difference between the vacuum potential near the surface and the metal Fermi level. For Al(001), we obtained a value of 4.0 eV for an experimental value of 4.20 eV.⁴² The same test was employed for $\theta\text{-Al}_2\text{Cu}$ (001) surface and we concluded that a slab of seven metallic layers was sufficient to reproduce the electronic features of the metal. For this surface, the work function value is 4.1 eV in good agreement with the value of 4.2 eV in the literature.⁴³

Results

Models.— $\text{Al}_2\text{Cu}(001)$ surface.—The study of the Al_2Cu intermetallic growth and solidification has been the subject of several works.^{44–51} In, particular, the $\theta\text{-Al}_2\text{Cu}$ phase has attracted a lot of attention due to its formation in every AlCu alloys. The first studies on Al_2Cu compound were conducted by Friauf.⁵² He described Al_2Cu as a tetragonal crystal of 14/mcm space group. Then, Jiang et al.⁴⁹ showed that the $\theta\text{-Al}_2\text{Cu}$ formation is controlled by atomic diffusion at the interfaces and grain boundaries. Chen et al.⁵³ demonstrated by scanning tunnelling microscopy that the first phase to form is the tetragonal $\theta\text{-Al}_2\text{Cu}$ one, due to its lowest formation energy. Haidara et al.⁵⁴ reported that the intermetallic phase composition is formed regardless of the alloy initial composition. Furthermore, the preferential directions of dendrite growth have attracted great interest.^{55–59} These studies have shown that the alloy solidification direction does not depend solely on the composition but also solidification parameters such as the temperature gradient for example.^{60,61} Thus literature agrees today on a $\theta\text{-Al}_2\text{Cu}$ preferential orientation surface in the direction [001].^{62,63}

Bulk $\gamma\text{-Al}_2\text{O}_3$.—In a first step, we examined the Al and Al_2Cu structures and built surfaces with unit cells of similar sizes. The (3×3) Al(001) surface (dimensions 12.15×12.15 Å²) is close to the (2×2) Al_2Cu (001) surface cell dimension (11.96×11.96 Å²), as the cell dimensions differ by only 1.56%. For Al_2Cu , we considered a Cu- and an Al- terminated surface. A seven (respectively eight) metal layer slab was considered for Cu (respectively Al)-terminated Al_2Cu surface, with five bottom layers frozen. A seven layer slab with five frozen bottom layers was considered for Al(001). The calculated work functions were 4.0, 3.9 and 4.1 for Al(001), $\text{Al}_2\text{Cu}\text{-Al}$ and $\text{Al}_2\text{Cu}\text{-Cu}$, respectively, in good agreement with literature.^{2,21}

The second step consisted in the construction of an oxide cell, that could model the Al_2O_3 layer on Al_2Cu and Al(001). We did not find any reference on epitaxy relationships between Al_2O_3 and Al_2Cu . We can consider as an example of epitaxial relationship, the $\text{Al}_2\text{O}_3/\text{Ti}$ interface, with a lattice mismatch of 7.5%.⁶⁴ An epitaxial $\text{Al}_2\text{O}_3/\text{SnO}_2$ interface was also produced with a mismatch of 11.52%.⁶⁵ Based on those experimental examples, we tried to build an epitaxy relationship with a mismatch less than 10%.

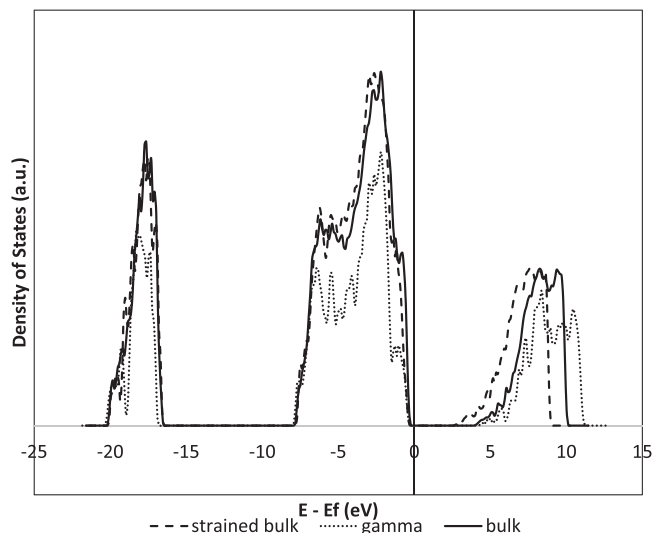


Figure 1. Projected Density of States of bulk aluminas: γ' - Al_2O_3 (plain black line), strained γ' - Al_2O_3 (- - dashed black line) and γ - Al_2O_3 (-plain grey line). The Fermi level is set at the origin of the energies (in eV). Snapshot on the [0, 5] eV zone, on the bottom of the conduction bands.

We thus built a bulk Al_2O_3 supercell that could fit with the (3×3) $\text{Al}(001)$ and (2×2) $\text{Al}_2\text{Cu}(001)$ cells. The c direction of Al_2O_3 is 5.55 Å, giving 11.1 if multiplied by two, and can be used to fit one of the metal surface directions. The cell value is $a = 8.03$ Å, and multiplied by 3 it gives 24.09 Å. Thus, a (2×3) Al_2O_3 (010) cell of dimensions (11.1×24.09) Å² was built. This allows us to obtain a good fit with $\text{Al}/\text{Al}_2\text{Cu}$, with a cell size of (12.15×24.3) Å² for Al and (11.96×23.92) Å² for Al_2Cu . In such cells, the mismatch between γ - $\text{Al}_2\text{O}_3(010)$ and $\text{Al}(001)$ and the mismatch between γ - $\text{Al}_2\text{O}_3(010)$ and $\text{Al}_2\text{Cu}(001)$ is 9 and 7%, respectively, in the b direction, and negligible (less than 1%) in the a direction. With this cell, we built four surfaces: $\text{Al}(001)$, $\text{Al}_2\text{Cu}(001)$, γ - $\text{Al}_2\text{O}_3(010)/\text{Al}(001)$ and γ - $\text{Al}_2\text{O}_3(010)/\text{Al}_2\text{Cu}(001)$.

Calculations with such cells are intensive and do not allow a large number of calculations. Therefore, in order to perform more calculations on a system that is easier to handle, we built another oxide phase, named γ' - Al_2O_3 . The details for the construction are reported in SI-1 section. The new, γ' - Al_2O_3 bulk has a composition $\text{Al}_{48}\text{O}_{72}$, and the following cell parameters, $a' = 11.73$ Å, $b' = 8.8$ Å and $c' = 11.57$ Å (the cell size of γ - are $a = 8.03$ Å, $b = 8.34$ Å and $c = 5.55$ Å) for γ - Al_2O_3 (Fig. SI-1). It is important to verify if the electronic properties of the γ -alumina are maintained after the construction of the γ' phase. Figure 1 reports the density of states (DOS) of the bulk γ' - Al_2O_3 in comparison with the bulk γ - Al_2O_3 . We notice that the valence bands and conduction bands are identical. The conduction bands of the γ - and γ' - Al_2O_3 have a maximum at 8.3 eV, in good agreement with the experimental values 7–8 eV.^{66–68} The bottom of the conduction bands is at 4.1 and 3.95 eV above the Fermi level, for the γ - and γ' - Al_2O_3 respectively, confirming that both phases have similar electronic properties. The calculated gap, 4 eV, is in agreement with previous theoretical works.^{39,55,69} This band gap is much lower than the experimental value (7–8 eV), a known shortcoming of pure GGA.^{70,71}

The new γ' phase allowed us to build metal/oxide interfaces with a smaller mismatch: 4.7% for Al and 3% for Al_2Cu (see SI-1–2 section). We also plotted in Fig. 1 the bulk γ' to which the strain to accommodate the Al_2Cu cell was imposed. We observe a gap narrowing to 3.5 eV. As stated previously,⁶⁷ the difference in the gap values is due to the shift of the bottom of the conduction band.

From the γ' bulk, the (010) surface was constructed (see Fig. SI-2 in SI section). The Al_2O_3 (010) slab is stoichiometric. At the surface, the Al atoms are three fold coordinated, the oxygen are two-fold coordinated. The average Bader charge of the bulk O- atoms is

–1.63, and the charge of the surface O atoms is –1.59. The average Bader charge of bulk Al is 2.44, and 2.42 at the surface.

Ultrathin γ' - Al_2O_3 on Al and Al_2Cu .—From the γ' -oxide bulk, the γ' - Al_2O_3 surface (010) surface was built. In all cells, the oxide layer is 9 Å thick. Figure 2 shows the different models. The obtained oxide layers are of similar structure as without substrate, and are similar for both cell sizes. We calculated binding energies of the oxide/metal of 0.07 eV Å² (1.1 J m⁻²) for the γ' - $\text{Al}_2\text{O}_3/\text{Al}_2\text{Cu}-\text{Cu}_{\text{term}}$ interface, and slightly higher binding energies on Al terminated surfaces, 0.08 eV Å² (1.3 J m⁻²) for γ' - $\text{Al}_2\text{O}_3/\text{Al}$ and 0.10 eV Å⁻² (1.6 J m⁻²) for γ' - $\text{Al}_2\text{O}_3/\text{Al}_2\text{Cu}-\text{Al}_{\text{term}}$. These values agree well with the calculated value of 1.4 J m⁻² for $\text{Al}_2\text{O}_3/\text{Cu}(111)$.⁷² The higher adhesion energy of $\text{Al}_2\text{O}_3/\text{Al}$ and $\text{Al}_2\text{O}_3/\text{Al}_2\text{Cu}-\text{Al}_{\text{term}}$ with respect to $\text{Al}_2\text{O}_3/\text{Al}_2\text{Cu}-\text{Cu}_{\text{term}}$ is explained by the higher charge transferred from the metal to the oxide.⁷³

Work functions of γ' - $\text{Al}_2\text{O}_3(010)/\text{Al}(001)$ and effect of interfacial layer composition.

Surface terminations, composition and structure play an important role in the work function (Φ). The presence of an oxide layer and the composition of the metallic planes under the oxide layer modify Φ .^{3,6} In this section, we study the influence of Cu segregation underneath the oxide layer on the Φ value. To better characterize the interface, we studied, in addition to Cu , the influence of metals of increasing work function, Mg , Ag , Ni , Au , located at the Al surface or at the metal/oxide interface, on the resulting work function. The surface Al metallic plane is substituted by different metals (the M terminated surfaces are noted here $\text{Al}-\text{M}_{\text{term}}$ and the oxidized surfaces are noted $\text{Al}_2\text{O}_3/\text{Al}-\text{M}_{\text{term}}$). We note no effect of the M_{term} nature on the average oxide relaxation, and a small effect on the relaxation at the M_{term} -oxide interface. All the atomic densities in the metal/oxide interfacial region are given in Supp section SI-1–3. We observe that the M_{term} /oxide interfaces are sharp, with the exception of the $\text{Al}-\text{Mg}-\text{Al}_2\text{O}_3$ system, where a small fraction of Mg (0.67 at nm⁻²) has relaxed into the Al_2O_3 interface layer.

The different calculated Φ are compared to the experimental work function of each substitution metal. The experimental work functions are 3.66 eV for Mg (polycrystalline), 4.20 for $\text{Al}(001)$, 4.74 eV for $\text{Ag}(001)$, 5.10 eV for $\text{Cu}(001)$, 5.35 eV for $\text{Ni}(001)$ and 5.47 eV for $\text{Au}(001)$.^{19,74–76}

For the non-oxidized surfaces, we observe a moderate increase of the work function with increasing the work function of the metal replacing Al at the metal surface (Fig. 3a, $\Phi(\text{Al}-\text{M}_{\text{term}})$), blue points) from 4.0 for Mg to 4.6 eV for Au . The presence of the oxide, which, for each metal, increases Φ , reinforces this tendency (Fig. 3a, $\Phi(\text{Al}_2\text{O}_3/\text{Al}-\text{M}_{\text{term}})$ curve, orange points), as the $\Delta\Phi$ increases with $\Phi(\text{M}_{\text{term}})$, from Mg to Ni (Fig. 3a, $\Delta\Phi(\text{Al}_2\text{O}_3/\text{Al}-\text{M}_{\text{term}})$ curve, grey points). A Bader charge analysis reveals a charge transfer from the metal to the Al_2O_3 oxide (Fig. 3b, $\Phi(\text{Al}-\text{M}_{\text{term}})$ curve and $\Phi(\text{Al}_2\text{O}_3/\text{Al}-\text{M}_{\text{term}})$). The transferred charge originates mainly from the M_{term} layer, as will be detailed later.

Work functions of γ' - $\text{Al}_2\text{O}_3(010)/\text{Al}_2\text{Cu}(001)-\text{Cu}$ terminated surface and effect of metal termination.

The same study was performed for the $\text{Al}_2\text{Cu}(001)-\text{Cu}$ surfaces, which have been shown experimentally to be stabilized as a consequence of the preferential Al oxidation.³³ The surfaces are noted here $\text{Al}_2\text{Cu}-\text{M}_{\text{term}}$. As in the case of the oxidized Al systems, the metal/oxide interfaces are sharp for the Au , Ag and Ni interfaces, but the Cu , Al and Mg interfaces are smoother, the relaxation of the oxide and of the interface layer inducing a degree of mixing. For Al_{term} and Mg_{term} , 3.3% of the oxygen of the oxide make a bond either with the M_{term} . For Cu_{term} , the same amount of oxygen binds with an Al from the first Al plane under Cu , that has relaxed into the Cu plane. Finally, we notice that, in the case of Al_2Cu , the Cu , Al and Mg /oxide interfaces are smoother than their equivalent for Al .

The work functions calculated for the $\text{Al}_2\text{Cu}-\text{M}_{\text{term}}$ surfaces are reported in Fig. 4a. We observe the same tendencies as on the pure Al surface. The higher $\Phi(\text{M}_{\text{term}})$, the higher is $\Phi(\text{Al}_2\text{Cu}-\text{M}_{\text{term}})$.

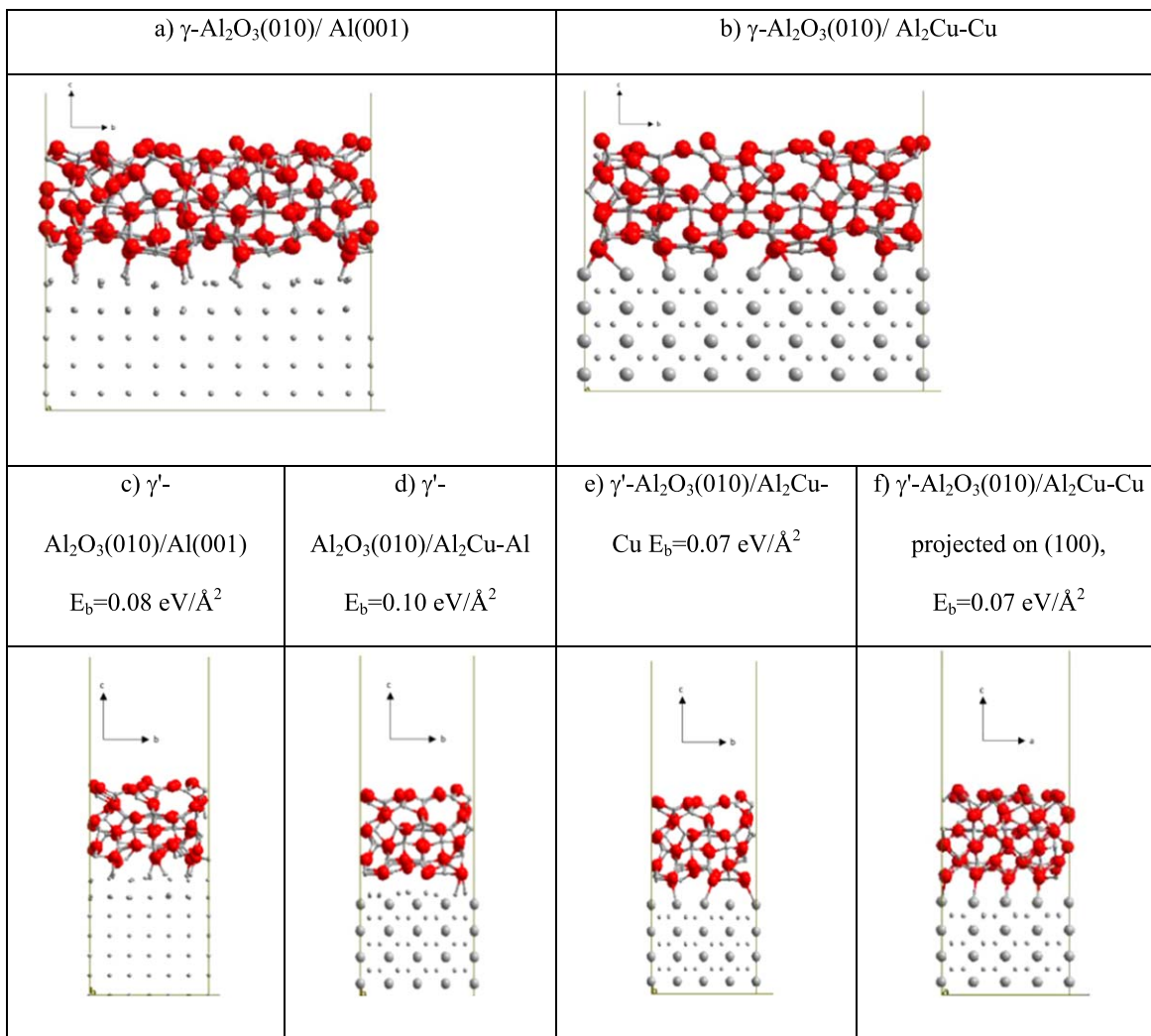


Figure 2. Optimized models of Al and Al₂Cu covered with an Al₂O₃ oxide layer (projection in the (010) plane, except for the bottom right, projection in the (100) plane) and binding energies of the γ '-Al₂O₃-oxide. Colour code: pink: Al; green: Cu; red: O.

Again, for each metal, the oxide layer increases Φ (see for a given M_{term} the blue and orange values) (Fig. 4a). Figure 4a also shows that the higher $\Phi(M_{\text{term}})$, the larger is $\Delta\Phi$. Figure 4b shows that again, the charge transferred to the oxide (due to the oxidation of M_{term}) increases (in absolute value) with increasing M_{term} work function.

M_{term} charge analysis.—Figure 5a shows that whereas an electron transfer is observed from Mg to the substrate, no significant charge transfer is observed between Mg and Al and the substrate (Al or Al₂Cu), whereas a significant electron transfer from the substrate to the terminal metal is observed for the more electronegative metals (Ag to Au).

Figure 5b reports the M_{term} charges on oxidized Al and Al₂Cu. The presence of the Al₂O₃ oxide induces an increase in the oxidation degree of Mg and Al, whereas no significant difference in the oxidation degree of the more electronegative metals is observed before and after oxidation. To summarize, a significant electron transfer occurs from Mg to Al or Al₂Cu, whereas the electron transfer is from Al or Al₂Cu to the more electronegative metals. The presence of Al₂O₃ layer induces an oxidation of Mg and Al, but no significant change of the charge of the other metals, which are obviously less easily oxidized.

Valence and conduction bands of the Al₂O₃ ultrathin layers above Al(001) and Al₂Cu(001) surfaces.—We study now the Valence

band (VB) and Conduction band (CB) positions of Al₂O₃ on Al and Al₂Cu. The electronic density of states (DOS) projected on the Al₂O₃ layers above the different metal surfaces are shown in Fig. 6 for Al and Al₂Cu with various M_{term} . All the data are reported in Table I.

We first observe that the VB maxima and VB edges (energy value below the Fermi level where the VB starts), which consist in Al3p and O2p bands (see the SI-2 section),⁷⁷ are shifted to lower energies (meaning that the Schottky barrier is higher) when passing from the more electronegative to the less electronegative metal, both on Al and Al₂Cu (Table I and Fig. 6). This increase in the Schottky barrier with decreasing metal electronegativity was already mentioned for Al₂O₃ thin films on pure metals (Ni, Cu) and on Cu–Al and Ni–Al alloys, where the VB starts at 1.4 eV and 2 eV below E_f for Al₂O₃/Ni–Al and Al₂O₃/Cu–Al, respectively.⁷⁸ Other authors calculated a value of 2.3 eV for the VB maximum of α -Al₂O₃/Cu(111).⁷² This last value agrees well with our calculated value of 2.2 eV for the Al–Cu system.

As for the VB maxima, we calculate a VB at 4.2 eV for Al₂O₃/Al, and a lower value, 3.2 eV, when the underlying metal plane is enriched in Cu. On Al₂Cu, the $V_{B_{\text{max}}}$ is at 4.28 on the Al terminated surface and 3.78 eV on the Cu one. This decrease of VB maximum was observed when comparing Al₂O₃ on pure Cu (3.2 eV) and Al₂O₃ on Cu-9Al, Al terminated (4.4 eV).⁷⁸ The experimental value of 3.5 eV was measured on Al(431) substrate after thermal oxidation.⁷⁹ Figure 6 confirms that, for Al and for Al₂Cu, $V_{B_{\text{max}}}$ increases with decreasing M_{term} work function.

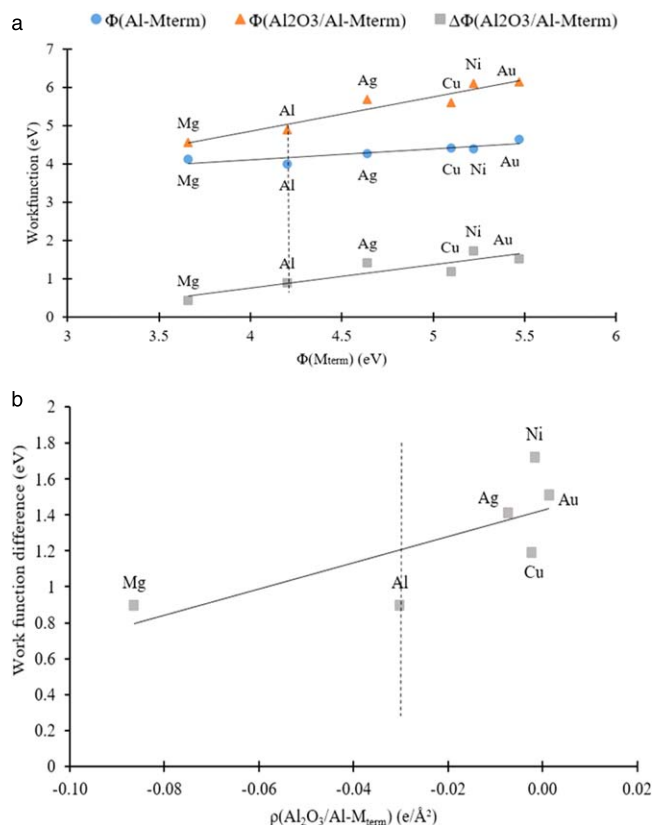


Figure 3. (a) Work function (Φ) calculated for the metallic ($Al-M_{term}$) and Al_2O_3 -oxide covered ($Al_2O_3/Al-M_{term}$) $Al(001)$ surface, and work function difference ($\Delta\Phi$) with respect to the non-oxidized surface, plotted vs the experimental Φ value of the terminating metal (Mg, Al, Ag, Cu, Ni, Au), (b) work function difference ($\Delta\Phi$), plotted vs the density of charge transferred to the oxide. The dashed line indicate data for pure Al.

The energy level of the conduction band (CB) also varies with the nature of M_{term} , and for Al and Al_2Cu , the CB value increases with increasing the M_{term} work function. In consequence, the acceptor states of the oxide on Cu-terminated metal are higher, suggesting a lower reactivity of the oxide (higher protection power against electron transfer, and, possibly, corrosion). As for the gap value, a slight gap opening is calculated with increasing M_{term} work function.

Application to the systems of interest for corrosion.—In the preceding part, we have shown that the work function increases with

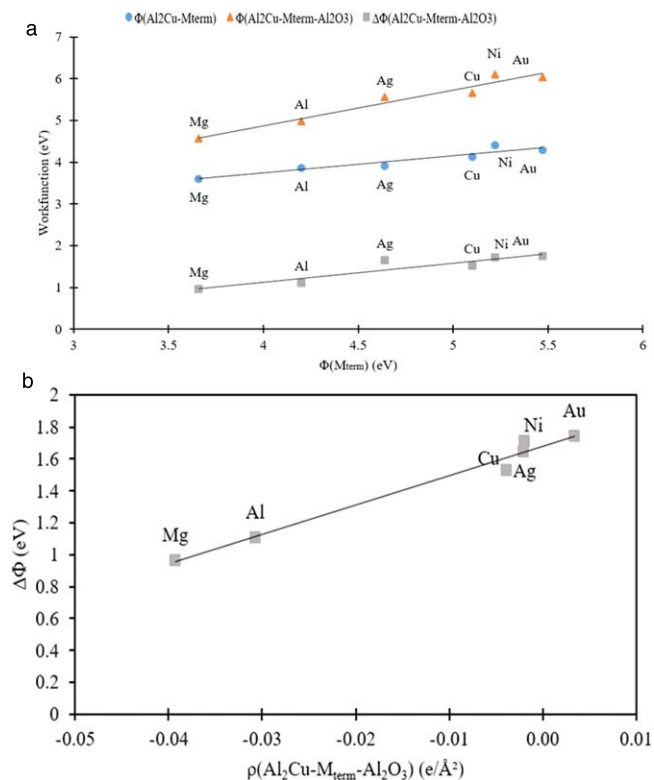


Figure 4. Work function (Φ) calculated for the metallic M_{term} and Al_2O_3 -oxide covered Al_2Cu surface, and work function difference ($\Delta\Phi$), plotted vs (a) the experimental Φ value of M_{term} (Mg, Al, Ag, Cu, Ni, Au), (b) the density of charge transferred to the oxide.

the presence of the Al_2O_3 oxide layer and with the increasing nobility of the metal underneath the oxide film, and that the determining parameter for the Φ value change is the charge transferred to the oxide, hence the oxidation degree of the metallic plane underneath the oxide. We have also found that the electronic gap slightly increases, whereas the Schottky barrier becomes lower with increasing metal work function. Now, we will consider the systems which are the most relevant for the characterization of the surface properties of Al–Cu alloys and Al_2Cu intermetallic particles. Figure 7 summarizes the results for Al, Al– Cu_{term} , Al_2Cu-Al_{term} and Al_2Cu-Cu_{term} .

The work function is in both cases higher for Al_2Cu than for pure Al. In average, the Schottky barriers are higher for Al_2Cu than for Al, but due to the influence of the interfacial plane nature, no simple trend can be drawn. Finally, the gap values are higher for Al_2Cu

Table I. Summary of the calculated electronic properties (work function, Φ , conduction band, CB, valence band edge VB_{edge} , valence band maxima VB_{max}) of the $\gamma-Al_2O_3$ film as a function of the underlying metal and interface plane composition.

Supporting Metallic Phase	Mterm	Φ (eV)	CB (eV)	VB_{edge} (eV)	VB_{max} (eV)	Gap(eV)
Al(001)	Mg	4.6	1.1	1.94	4.32	3.04
	Al	5.1	1.29	1.72	4.18	3.01
	Cu	5.4	2.20	1.0	3.25	3.2
	Ag	5.7	2.3	0.87	3.21	3.17
	Ni	6.4	2.1	0.98	3.27	3.02
	Au	6.1	2.6	0.50	2.89	3.11
$Al_2Cu(001)$	Mg	4.6	0.87	2.64	4.89	3.5
	Al	5.4	1.83	2.05	4.28	3.53
	Cu	5.7	2.34	1.42	3.78	3.60
	Ag	5.5	2.27	1.2	3.95	3.47
	Ni	6.1	1.19	1.19	3.40	3.77
	Au	6.0	0.65	0.65	3.24	3.63

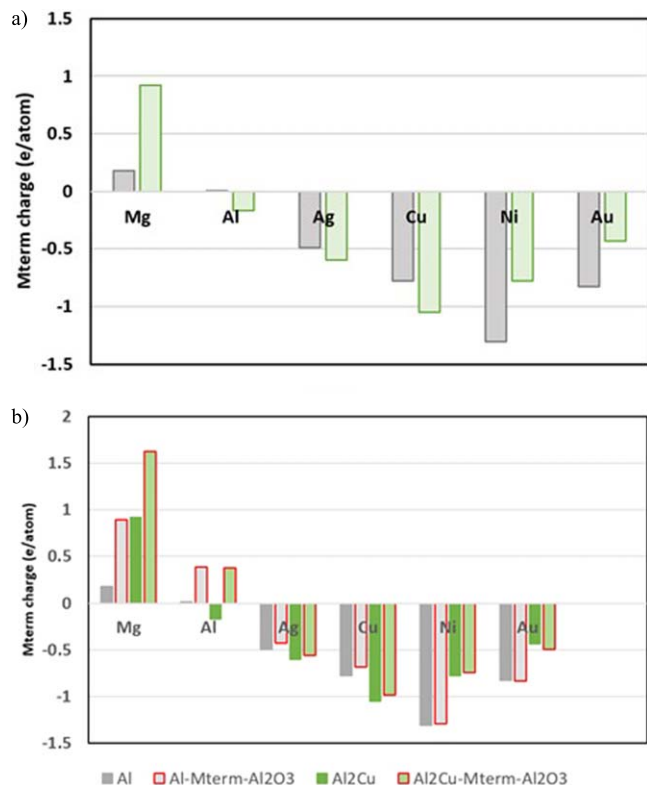


Figure 5. (a) M_{term} charge on Al (grey) and Al_2Cu (green); (b) M_{term} charge on the metal and oxidized surfaces. Colour code: grey: Al; grey with a red line: Al-M_{term}-Al₂O₃; green = Al₂Cu and green with a red line: Al₂Cu-M_{term}-Al₂O₃

(3.5–3.6 eV) than for Al (3.1–3.2 eV), suggesting a lower reactivity of the oxide film on Al₂Cu than on Al.

In addition to the slabs with γ' -Al₂O₃, the Al/Al₂O₃ and Al₂Cu-Cu_{term} systems were optimized in large cells, with the γ' -Al₂O₃ over the surface (see section 3.1.2 and Fig. 2). Table II summarizes the work function values of the studied systems. We observe that the calculated Φ are in the same range as those calculated with the γ' -Al₂O₃ layer: we find a Φ value of 5.3 eV for Al(001)/ γ' -Al₂O₃ (100) (to be compared to 5.1 eV for the γ' analog), and 6.2 eV for Al₂Cu(001)-Cu/ γ' -Al₂O₃ (100), (5.7 eV for the γ' analog), confirming the higher Φ of oxidized Al₂Cu(001)-Cu with respect to oxidized Al.

On pure Al, Cu segregation increases Φ by 0.3–0.4 eV, whereas the effect of oxide layer on Φ is higher (1–1.3 eV). In other words, the first parameter influencing the Φ value on Al is the presence of an oxide layer, the metallic composition under the oxide film having also a significant, but less pronounced effect. The same trend is observed for Al₂Cu: the Cu termination gives a higher Φ than the Al one, by 0.3–0.4 eV, and the presence of oxide significantly increases the Φ values, by 1.4–2.1 eV.

Thus, for Al₂Cu as for Al, two factors determine the value of Φ : the presence of an oxide layer (increase by more than 1 eV) and the composition of the metallic plane under the oxide film (increase of 0.3 eV when Cu is present under the oxide film instead of Al).

Potential drop at the Al(010)//Al₂Cu(010) interface.—We now consider the two combined models, i.e. the Al(010)//Al₂Cu(010) interface, and the (001) surface, covered or not with an Al₂O₃ oxide layer. The Al(010)//Al₂Cu(010) semi coherent interface was observed experimentally.^{30,80} Here we compare the potential drop at the Al//Al₂Cu interface, without and with an oxide layer. We choose the Al-Cu and Al₂Cu-Cu terminated surfaces as the most relevant, considering our previous findings,³³ using XPS and ToF-SIMS

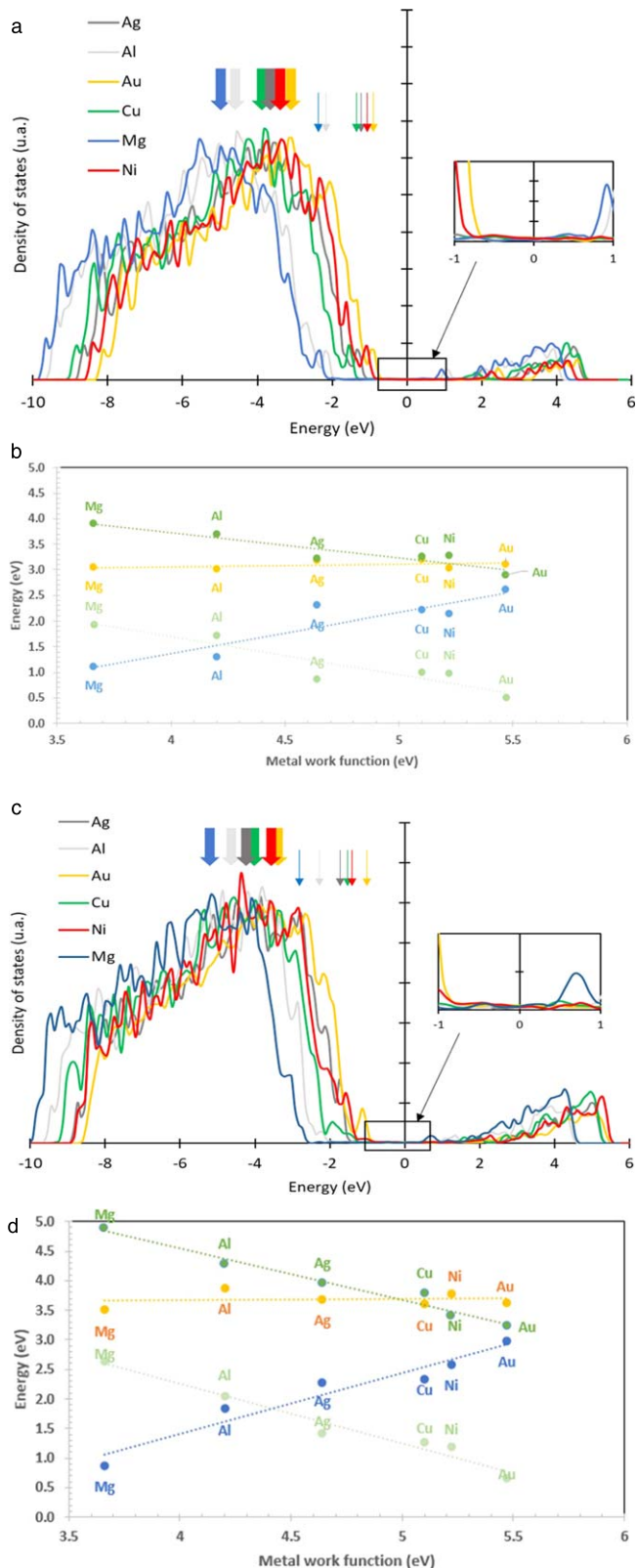


Figure 6. Projected DOS and energy values for the Valence band maxima (dark green), valence band edges (light green), conduction band (blue), and gaps, (orange) of the Al₂O₃ oxide supported on (a)–(b) Al(010), (c)–(d) Al₂Cu(001), with different metals termination (Insets in the DOS are for visibility). Arrows indicate the VB_{max} and VB edges. Snapshots on the region near the Fermi energy. The zero is set at the Fermi level. The colour code for the metals in the projected DOS are: Orange: Au, red: Ni, dark grey: Ag, green: Cu, light grey: Al, blue: Mg.

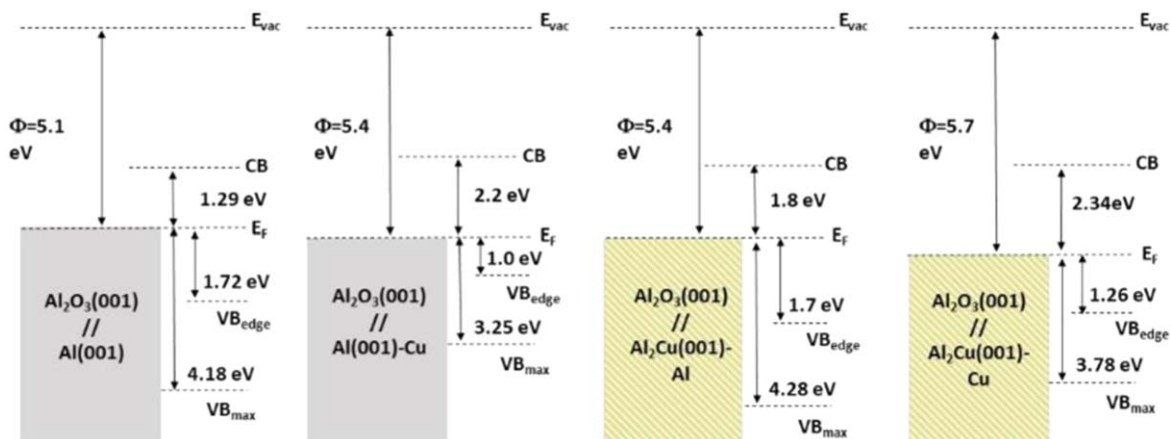


Figure 7. Electronic level diagrams calculated for Al and Al₂Cu covered with Al₂O₃, with Cu or Al termination. E_{vac} and E_f are the energy levels of the vacuum, and of the Fermi level, respectively. CB refers to the conduction band, VB to the valence band. Φ is the work function.

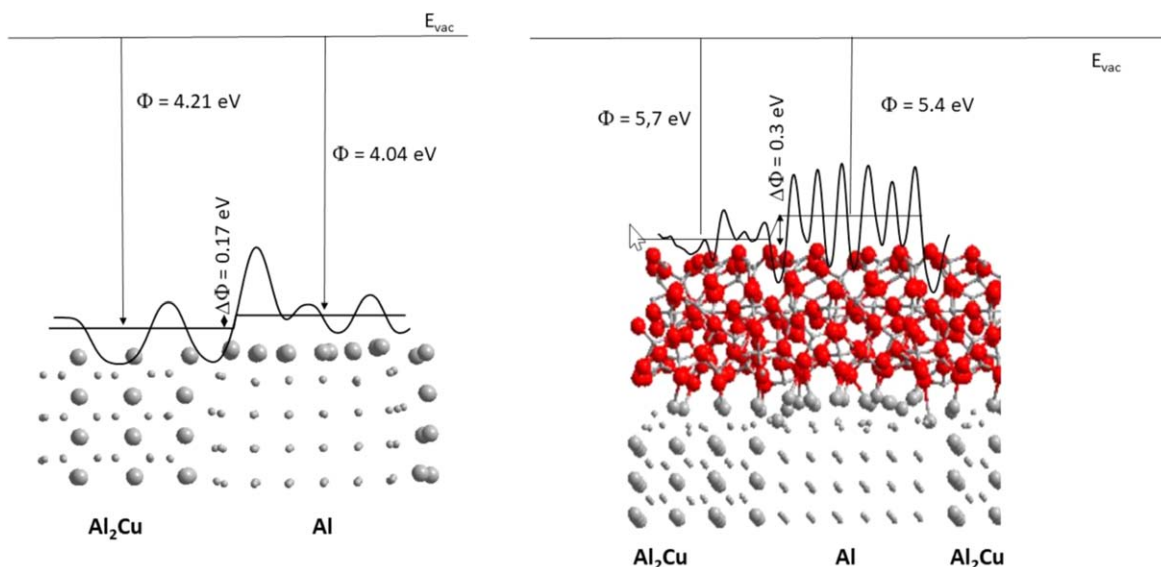


Figure 8. Electrostatic potential variation at the (001) surfaces of the Al(010)//Al₂Cu(010) interface, (a) metal and (b) oxidized surface. Al and Cu are grey (small: Al; large: Cu), O is red.

analyses, that copper segregates at the metal/oxide interface on both intermetallic particles and aluminium matrix. We reproduce this interface, without (Fig. 8a) and with (Fig. 8b) the oxide layer. We can thus model the potential drop at the interface. We take as the potential drop the difference between the average values from both sides of the interface. We considered that the potential drop is equal to the work function difference, according to equation $\Delta\Psi = \Delta\Phi/e$ ²¹ and found that $\Delta\Psi \sim 170$ mV and 300 mV for the non-oxidized and oxidized surfaces, respectively, where the Al₂Cu part is always the more noble (see Fig. 8). It should be pointed out that the model used is of very small size, and thus boundary effects are important. However, this simple case confirms that the Volta potential of the IMP is higher than that of the matrix, (covered or not with oxide, provided the oxide has the same thickness).

Discussion

It is now possible to gather all the available data from the present work, and data from literature, and try to propose a rational discussion of the role of the surface terminations of Al₂Cu//Al on the work function values.

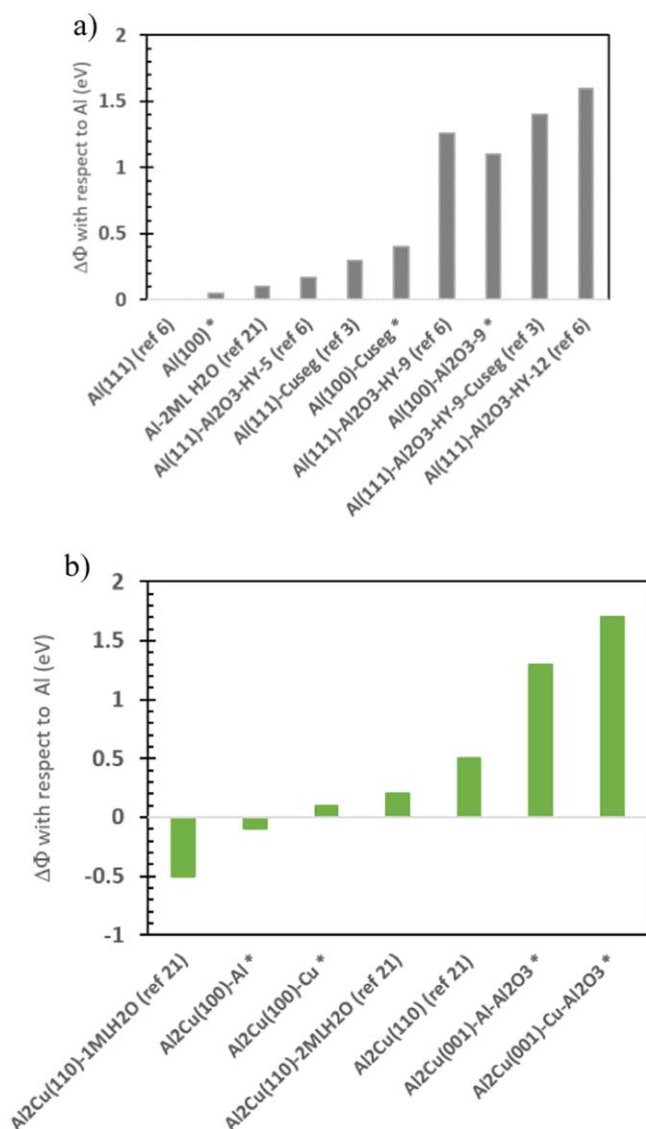
The present theoretical data are first compared to other published data. As explained in the introduction, few theoretical works have

been performed on Al₂Cu systems, and it is worth combining all results. Indeed, we studied in a previous work the influence of the oxide thickness on the work function Φ ⁶. In this work, we showed that the work function increases with increasing oxide thickness, and that the oxide recovers the electronic properties of the bulk for a thickness of 1.2 nm. We also studied the influence of Cu segregation at the Al(111) surface,³ in the presence of an oxide layer, and showed that a fraction of Cu monolayer leads to an increase in the work function. More recently Leygraf et al. modelled the adsorption of water at Al and Al₂Cu surfaces.²¹ Water adsorbed at the metal surface can represent a model of the metal surface in interaction with an aqueous solution, or of the first stage of an oxide growth.

Figure 9 shows the computed $\Delta\Phi$ (assimilated to the Volta potential difference, as $\Delta\Psi = \Delta\Phi/e$) with respect to the Al metal surface. All data are detailed in the SI-3 section (Table SI-II). Figure 9a shows that the presence of adsorbed water has little influence on Φ_{Al} for Al(111). An ultrathin oxide layer (5 Å) induces a Φ increase of 0.2 eV, comparable to water adsorption. Thicker oxides (from 9 to 12 Å), induce a significant increase in Φ (1–1.6 eV).⁶ Cu segregation at the Al(001) surface, induces a moderate increase of Φ , (0.3–0.4 eV, this work). We note that for Al₂O₃(111)/Al(111), the opposite effect was found, the Cu segregation inducing a lowering of the work function value of -0.3 eV, due

Table II. Work function Φ (eV) and gap (eV) calculated for the different models of metal/intermetallic compound without and with a γ or γ' - Al_2O_3 oxide layer, work function differences ($\Delta\Phi$) with respect to the non-oxidized surface or to the surface without Cu.

Metallic Phase	Surface composition Termination	Φ (eV)	Effect of Cu on Φ (eV)	Effect of oxide on Φ (eV)
Al(001)	Al(001)	4.0		
	Al(001)/ γ - Al_2O_3 (100)	5.3		+1.3
	Al(001)/ γ' - Al_2O_3 (100)	5.1		+1.1
	Al(001)- Cu_{seg}	4.4	+0.4	
Al_2Cu (001)	Al(001)- $\text{Cu}_{\text{seg}}/\gamma'$ - Al_2O_3 (100)	5.4	+0.3	+1.0
	Al_2Cu (001)/Al	3.9	+0.3	
	Al_2Cu (001)/Al/ γ' - Al_2O_3 (100)	5.3		+1.4
	Al_2Cu (001)-Cu	4.1	—	
	Al_2Cu (001)-Cu/ γ' - Al_2O_3 (100)	5.7	+0.4	+1.6
	Al_2Cu (001)-Cu/ γ - Al_2O_3 (100)	6.2	—	+2.1

**Figure 9.** Work function differences (eV) with respect to pure metal Al(111) for (a) Al models with data from Refs. 3, 6 and 21 and from this work, (b) Al_2Cu models with data from Ref. 21 and from this work. “HY”: hydroxylated surface. Details about all data are in SI section SI-3. The data provided by the present work are indicated by an *.

to a charge transfer from the oxide layer to the metal interface.³ We attribute this difference to the polar character of γ - Al_2O_3 (111), for which the interfacial plane is in contact with a full oxygen layer.

As mentioned previously, it is found that the most important factor governing the Φ value for Al is the presence of an oxide layer. Segregation of Cu is the second determining factor, and water adsorption on the metal surface has only a weak effect on Φ .

The trends are identical for Al_2Cu , (see Fig. 9b), with water adsorption having a small effect on Φ , the nature of the metal under the oxide film having an effect of up to 0.5 eV, and the presence of an oxide film inducing the largest increase of 1.4–1.6 eV.

We can finally compare the calculated results with experimental measurements⁸¹ of Volta potential for Al and Al_2Cu before immersion in aqueous solution, which correspond best to the native oxide analysed in our previous paper on a model Al–Cu alloy.³³ The authors⁸¹ report that the Al_2Cu surface Volta potential is more noble by 0.2 V than the Al matrix. This result is in good agreement with our own calculations ($\Delta\Phi = 0.3$ eV, see Fig. 7).

Conclusions

DFT calculations of Al and Al_2Cu covered by the same Al_2O_3 oxide layer have been performed, allowing us to study two parameters influencing the metal/alloy electronic properties: the presence of an ultrathin oxide layer and the composition of the first metallic plane under the oxide film. The main results are the following:

- A model for Al_2Cu intermetallic covered by an ultrathin Al_2O_3 oxide layer is proposed, which is, to the best of our knowledge, the first atomistic model of (pre)oxidized Al_2Cu .
- A commensurate Al(010)// Al_2Cu (010) interface, covered by an ultrathin oxide layer, was built.
- The presence of the oxide layer increases the work function Φ of Al and Al_2Cu surfaces by 1–1.6 eV, and the presence of Cu under the oxide film also increases the work function, with however a less marked effect (~ 0.3 eV).
- A systematic study of the effect of different metals (Mg, Al, Cu, Ag, Ni, Au) segregated at the oxide-matrix interface, with metals of increasing work function, has shown that for both Al and Al_2Cu , the determining factor for the work function variation is the amount of charge transferred to the oxide by the oxidation of the interfacial metal layer.
- The work function difference between Al and Al_2Cu (0.2 eV) is maintained, and even reinforced, in the presence of the oxide layer.
- The same result was found on a model of Al(010)// Al_2Cu (010) interface terminated with the (001) surface.
- The relation between work function and Volta potential has been discussed.

Acknowledgments

GENCI is acknowledged for high performance calculations in the national (IDRIS, CINES) centers under the project c2016082217.

Pauline Cornette thanks the French Research Ministry for PhD grant.

CRedit Author Statement

P. Cornette: Investigation; Formal analysis, Writing; original Draft; Writing; review & Editing.

D. Costa: Supervision, Project Administration, Resources, Methodology, Investigation, Formal Analysis, Validation, Data Curation, Writing-Review & Editing.

P. Marcus: Conceptualization, Funding acquisition, Writing-Review & Editing.

ORCID

D. Costa  <https://orcid.org/0000-0002-3781-9867>

P. Marcus  <https://orcid.org/0000-0002-9140-0047>

References

- M. Liu, Y. Jin, C. Zhang, C. Leygraf, and L. Wen, "Density-functional theory investigation of Al pitting corrosion in electrolyte containing chloride ions." *Appl. Surf. Sci.*, **357 Part B**, 2028 (2016).
- Y. Jin, M. Liu, C. Zhang, C. Leygraf, L. Wen, and J. Pan, "First-principle calculation of volta potential of intermetallic particles in aluminum alloys and practical implications." *J. Electrochem. Soc.*, **164**, C465 (2017).
- P. Cornette, D. Costa, and P. Marcus, "DFT modelling of Cu segregation in Al-Cu alloys covered by an ultrathin oxide film and possible links with passivity." *Metals*, **7**, 366 (2017).
- D. Costa, T. Ribeiro, P. Cornette, and P. Marcus, "DFT modeling of corrosion inhibition by organic molecules: carboxylates as inhibitors of aluminum corrosion." *J. Phys. Chem. C*, **120**, 28607 (2016).
- T. Ribeiro, A. Motta, P. Marcus, M.-P. Gaigeot, X. Lopez, and D. Costa, "Formation of the OOH radical at steps of the boehmite surface and its inhibition by gallic acid: a theoretical study including DFT-Based dynamics." *J. Inorg. Biochem.*, **128**, 164 (2013).
- D. Costa, T. Ribeiro, F. Mercuri, G. Pacchioni, and P. Marcus, "Atomistic modeling of corrosion resistance: a first principles study of O₂ reduction on the Al(111) surface covered with a thin hydroxylated alumina film." *Adv. Mater. Interfaces*, **1**, 1300072 (2014).
- N. Li, C. Dong, C. Man, and J. Yao, "In situ electrochemical atomic force microscopy and Auger spectroscopy study on the passive film structure of 2024-T3 aluminum alloy combined with a density functional theory calculation." *Adv. Eng. Mater.*, **21**, 1900386 (2019).
- I. Milošev et al., "Electrochemical, surface-analytical, and computational DFT study of alkaline etched aluminum modified by carboxylic acids for corrosion protection and hydrophobicity." *J. Electrochem. Soc.*, **166**, C3131 (2019).
- I. Milošev et al., "Editors' choice—the effect of anchor group and alkyl backbone chain on performance of organic compounds as corrosion inhibitors for aluminum investigated using an integrative experimental-modeling approach." *J. Electrochem. Soc.*, **167**, 061509 (2020).
- M. Nezafati, K. Cho, A. Giri, and C.-S. Kim, "DFT study on the water molecule adsorption and the surface dissolution behavior of Mg alloys." *Mater. Chem. Phys.*, **182**, 347 (2016).
- C.-H. Zhang, M. Liu, Y. Jin, and D.-B. Sun, "The corrosive influence of chloride ions preference adsorption on α -Al₂O₃ (0001) surface." *Appl. Surf. Sci.*, **347**, 386 (2015).
- L. Marks, "Competitive chloride chemisorption disrupts hydrogen bonding networks: DFT, crystallography, thermodynamics, and morphological consequences." *Corrosion*, **74**, 295 (2018).
- A. Bouzoubaa, D. Costa, B. Diawara, N. Audiffren, and P. Marcus, "Insight of DFT and atomistic thermodynamics on the adsorption and insertion of halides onto the hydroxylated NiO(111) surface." *Corros. Sci.*, **52**, 2643 (2010).
- A. Bouzoubaa, B. Diawara, V. Maurice, C. Minot, and P. Marcus, "Ab initio study of the interaction of chlorides with defect-free hydroxylated NiO surfaces." *Corros. Sci.*, **51**, 941 (2009).
- M. Liu, Y. Jin, C. Leygraf, and J. Pan, "A DFT-Study of Cl Ingress into α -Al₂O₃ (0001) and Al(111) and its possible influence on localized corrosion of Al." *J. Electrochem. Soc.*, **166**, C3124 (2019).
- M. Liu, Y. Jin, J. Pan, and C. Leygraf, "Co-Adsorption of H₂O, OH, and Cl on aluminum and intermetallic surfaces and its effects on the work function studied by DFT calculations." *Molecules*, **24**, 4284 (2019).
- C. Örnek, C. Leygraf, and J. Pan, "On the volta potential measured by SKPFM—fundamental and practical aspects with relevance to corrosion science." *Corros. Eng. Sci. Technol.*, **54**, 185 (2019).
- A. Kokalj, "On the HSAB based estimate of charge transfer between adsorbates and metal surfaces." *Chem. Phys.*, **393**, 1 (2012).
- H. B. Michaelson, "Relation between an atomic electronegativity scale and the work function." *IBM J. Res. Dev.*, **22**, 72 (1978).
- K. P. Kepp, "Chemical causes of metal nobleness." *ChemPhysChem*, **21**, 360 (2020).
- C. Örnek, M. Liu, J. Pan, Y. Jin, and C. Leygraf, "Volta potential evolution of intermetallics in aluminum alloy microstructure under thin aqueous adlayers: a combined DFT and experimental study." *Top. Catal.*, **61**, 1169 (2018).
- S. Trasatti, "Surface science and electrochemistry: concepts and problems." *Surf. Sci.*, **335**, 1 (1995).
- M. Stratmann and H. Streckel, "The investigation of the corrosion of metal surfaces, covered with thin electrolyte layers—a new experimental technique." *Berichte Bunsenges. Für Phys. Chem.*, **92**, 1244 (1988).
- P. Schmutz and G. S. Frankel, "Characterization of AA2024-T3 by scanning Kelvin probe force microscopy." *J. Electrochem. Soc.*, **145**, 2285 (1998).
- Y. Zhu, K. Sun, and G. S. Frankel, "Intermetallic phases in aluminum alloys and their roles in localized corrosion." *J. Electrochem. Soc.*, **165**, C807 (2018).
- T. H. da Silva, E. B. Nelson, I. Williamson, C. M. Efav, E. Sapper, M. F. Hurley, and L. Li, "First-principles surface interaction studies of aluminum-copper and aluminum-copper-magnesium secondary phases in aluminum alloys." *Appl. Surf. Sci.*, **439**, 910 (2018).
- X. Zhang and Y. Zhang, "Effects of local geometry distortion at the Al/Al₂Cu interfaces on solute segregation." *Phys. Chem. Chem. Phys.*, **22**, 4106 (2020).
- Q. Zhou, D. P. Hua, Y. Du, Y. Ren, W. W. Kuang, Q. S. Xia, and V. Bhardwaj, "Atomistic study of atomic structures and dislocation nucleation at Al/Al₂Cu interfaces." *Int. J. Plast.*, **120**, 115 (2019).
- K. Kim, B.-C. Zhou, and C. Wolverton, "Interfacial stability of θ /Al in Al-Cu alloys." *Scr. Mater.*, **159**, 99 (2019).
- A. Biswas, D. J. Siegel, C. Wolverton, and D. N. Seidman, "Precipitates in Al-Cu alloys revisited: atom-probe tomographic experiments and first-principles calculations of compositional evolution and interfacial segregation." *Acta Mater.*, **59**, 6187 (2011).
- C. Lanthony, J. M. Ducéré, M. D. Rouhani, A. Hemeryck, A. Estève, and C. Rossi, "On the early stage of aluminum oxidation: an extraction mechanism via oxygen cooperation." *J. Chem. Phys.*, **137**, 094707 (2012).
- J. D. Baran, H. Grönbeck, and A. Hellman, "Mechanism for limiting thickness of thin oxide films on aluminum." *Phys. Rev. Lett.*, **112**, 146103-1 (2014).
- P. Cornette, S. Zanna, A. Seyeux, D. Costa, and P. Marcus, "The native oxide film on a model aluminum-copper alloy studied by XPS and ToF-SIMS." *Corros. Sci.*, **174**, 108837 (2020).
- J. P. Perdew, J. A. Chevary, S. H. Vosko, K. A. Jackson, M. R. Pederson, D. J. Singh, and C. Fiolhais, "Atoms, molecules, solids, and surfaces: applications of the generalized gradient approximation for exchange and correlation." *Phys. Rev. B*, **46**, 6671 (1992).
- J. P. Perdew, K. Burke, and M. Ernzerhof, "Generalized gradient approximation made simple." *Phys. Rev. Lett.*, **77**, 3865 (1996).
- G. Kresse and J. Hafner, "Ab initio molecular-dynamics simulation of the liquid-metal amorphous-semiconductor transition in germanium." *Phys. Rev. B*, **49**, 14251 (1994).
- P. E. Blöchl, O. Jepsen, and O. K. Andersen, "Improved tetrahedron method for Brillouin-zone integrations." *Phys. Rev. B*, **49**, 16223 (1994).
- G. Kresse and D. Joubert, "From ultrasoft pseudopotentials to the projector augmented-wave method." *Phys. Rev. B*, **59**, 1758 (1999).
- M. Digne, "Use of DFT to achieve a rational understanding of acid? Basic properties of γ -alumina surfaces." *J. Catal.*, **226**, 54 (2004).
- A. Benali, C. Lacaze-Dufaure, and J. Morillo, "Density functional study of copper segregation in aluminum." *Surf. Sci.*, **605**, 341 (2011).
- H. J. Monkhorst and J. D. Pack, "Special points for Brillouin-zone integrations." *Phys. Rev. B*, **13**, 5188 (1976).
- J. Hölzl and F. K. Schulte, "Work function of metals." *Solid Surface Physics*, ed. J. Hölzl, F. K. Schulte, and H. Wagner (Springer, Berlin, Heidelberg) **85**, 1 (1979).
- C. D. Yang, W. Li, and W. Zhi, "Study on mechanical behavior and electronic structures of Al-Cu intermetallic compounds based on first-principles calculations." *Solid State Commun.*, **151**, 1270 (2011).
- J. M. Vandenberg and R. A. Hamm, "An in situ X-ray study of phase formation in Cu-Al thin film couples." *Thin Solid Films*, **97**, 313 (1982).
- K. Rajan and E. R. Wallach, "A transmission electron microscopy study of intermetallic formation in aluminum-copper thin-film couples." *J. Cryst. Growth*, **49**, 297 (1980).
- C. J. Hang, C. Q. Wang, M. Mayer, Y. H. Tian, Y. Zhou, and H. H. Wang, "Growth behavior of Cu/Al intermetallic compounds and cracks in copper ball bonds during isothermal aging." *Microelectron. Reliab.*, **48**, 416 (2008).
- S. U. Campisano, E. Costanzo, F. Scaccianoce, and R. Cristofolini, "Growth kinetics of the θ phase in Al-Cu thin film bilayers." *Thin Solid Films*, **52**, 97 (1978).
- H. T. G. Hentzell, R. D. Thompson, and K. N. Tu, "Interdiffusion in copper-aluminum thin film bilayers. I. structure and kinetics of sequential compound formation." *J. Appl. Phys.*, **54**, 6923 (1983).
- H. G. Jiang, J. Y. Dai, H. Y. Tong, B. Z. Ding, Q. H. Song, and Z. Q. Hu, "Interfacial reactions on annealing Cu/Al multilayer thin films." *J. Appl. Phys.*, **74**, 6165 (1993).
- A. E. Gershinskii, B. I. Fomin, E. I. Cherepov, and F. L. Edelman, "Investigation of diffusion in the Cu-Al thin film system." *Thin Solid Films*, **42**, 269 (1977).
- H. T. G. Hentzell, R. D. Thompson, and K. N. Tu, "Motion of W Marker during sequential compound formation in bimetallic Al-Cu thin films." *Mater. Lett.*, **2**, 81 (1983).
- J. B. Friauf, "The crystal structures of two intermetallic compounds." *J. Am. Chem. Soc.*, **49**, 3107 (1927).
- C.-Y. Chen and W.-S. Hwang, "Effect of annealing on the interfacial structure of aluminum-copper joints." *Mater. Trans.*, **48**, 1938 (2007).
- F. Haidara, M.-C. Record, B. Duployer, and D. Mangelinck, "Investigation of reactive phase formation in the Al-Cu thin film systems." *Surf. Coat. Technol.*, **206**, 3851 (2012).

55. C. Li, H. Yang, Z. Ren, W. Ren, and Y. Wu, "Application of differential thermal analysis to investigation of magnetic field effect on solidification of Al-Cu hypereutectic alloy." *J. Alloys Compd.*, **505**, 108 (2010).
56. K. Gao, S. Song, S. Li, and H. Fu, "Characterization of microstructures and growth orientation deviating of Al₂Cu phase dendrite at different directional solidification rates." *J. Alloys Compd.*, **660**, 73 (2016).
57. K. Gao, S. Li, L. Xu, and H. Fu, "Effect of sample size on intermetallic Al₂Cu microstructure and orientation evolution during directional solidification." *J. Cryst. Growth*, **394**, 89 (2014).
58. F. Yilmaz and R. Elliott, "Faceting in the Al-CuAl₂ system." *J. Cryst. Growth*, **66**, 465 (1984).
59. K. Gao, S. M. Li, and H. Z. Fu, "Intermetallic Al₂Cu orientation and deviation angle measured by the rotating directional test during directional solidification." *Adv Mater Lett*, **2**, 368 (2011).
60. R. Hamar and C. Lemaignan, "Facetting behaviour of Al₂Cu during solidification." *J. Cryst. Growth*, **53**, 586 (1981).
61. R. Trivedi, S. Liu, P. Mazumder, and E. Simsek, "Microstructure development in the directionally solidified Al-4.0 Wt% Cu alloy system." *Sci. Technol. Adv. Mater.*, **2**, 309 (2001).
62. L. S. Loli, É. Gaudry, V. Fournée, M.-C. De Weerd, and J. Ledieu, "Dynamic structure mediated by graphitelike Al Nets on the Al₂Cu (001) surface." *Phys. Rev. Lett.*, **108**, 146101 (2012).
63. J. Ledieu, É. Gaudry, and V. Fournée, "Surfaces of Al-Based complex metallic alloys: atomic structure, thin film growth and reactivity." *Sci. Technol. Adv. Mater.*, **15**, 034802 (2014).
64. D. Rafaja, T. Schucknecht, V. Klemm, A. Paul, and H. Berek, "Microstructural characterisation of titanium coatings deposited using cold gas spraying on Al₂O₃ substrates." *Surf. Coat. Technol.*, **203**, 3206 (2009).
65. J. Lu, J. Sundqvist, M. Ottosson, A. Tarre, A. Rosental, J. Aarik, and A. Härsta, "Microstructure characterisation of ALD-grown epitaxial SnO₂ thin films." *J. Cryst. Growth*, **260**, 191 (2004).
66. B. Ealet, M. H. Elyakhloufi, E. Gillet, and M. Ricci, "Electronic and crystallographic structure of γ -Alumina thin films." *Thin Solid Films*, **250**, 92 (1994).
67. E. O. Filatova and A. S. Konashuk, "Interpretation of the changing the band gap of Al₂O₃ depending on its crystalline form: connection with different local symmetries." *J. Phys. Chem. C*, **119**, 20755 (2015).
68. S. Toyoda, T. Shinohara, H. Kumigashira, M. Oshima, and Y. Kato, "Significant increase in conduction band discontinuity due to solid phase epitaxy of Al₂O₃ gate insulator films on GaN semiconductor." *Appl. Phys. Lett.*, **101**, 231607 (2012).
69. F. Loviat, I. Czekaj, J. Wambach, and A. Wokaun, "Nickel deposition on γ -Al₂O₃ model catalysts: an experimental and theoretical investigation." *Surf. Sci.*, **603**, 2210 (2009).
70. V. Fiorentini and A. Baldereschi, "Dielectric scaling of the self-energy scissor operator in semiconductors and insulators." *Phys. Rev. B*, **51**, 17196 (1995).
71. J.-H. Yuan, Q. Chen, L. R. C. Fonseca, M. Xu, K.-H. Xue, and X.-S. Miao, "GGA-1/2 self-energy correction for accurate band structure calculations: the case of resistive switching oxides." *J. Phys. Commun.*, **2**, 105005 (2018).
72. R. Yang, S. Tanaka, and M. Kohyama †, "Chemical bonding at the Al-terminated stoichiometric α -Al₂O₃ (0001)/Cu(111) interface." *Philos. Mag. Lett.*, **84**, 425 (2004).
73. J.-G. Li, "Energetics of metal/ceramic interfaces, metal-semiconductor Schottky contacts, and their relationship." *Mater. Chem. Phys.*, **47**, 126 (1997).
74. J. Hölzl and F. K. Schulte, "Work function of metals." *Solid Surface Physics*, ed. J. Hölzl, F. K. Schulte, and H. Wagner (Springer Tracts in Modern Physics; Springer Berlin Heidelberg, Berlin, Heidelberg) 85, pp 1 (1979).
75. M. Green, "Solid state surface science." *Solid State Surface Science* (M. Dekker, New York) (1969).
76. H. B. Michaelson, "The work function of the elements and its periodicity." *J. Appl. Phys.*, **48**, 4729 (1977).
77. T. V. Perevalov, V. A. Gritsenko, and V. V. Kaichev, "Electronic structure of aluminum oxide: ab initio simulations of α and γ phases and comparison with experiment for amorphous films." *Eur. Phys. J. Appl. Phys.*, **52**, 30501 (2010).
78. M. Yoshitake, S. Nemšák, T. Skála, N. Tsud, T. Kim, V. Matolín, and K. C. Prince, "Modification of terminating species and band alignment at the interface between alumina films and metal single crystals." *Surf. Sci.*, **604**, 2150 (2010).
79. P. C. Snijders, L. P. H. Jeurgens, and W. G. Sloof, "Structure of thin aluminium-oxide films determined from valence band spectra measured using XPS." *Surf. Sci.*, **496**, 97 (2002).
80. A. Biswas, D. J. Siegel, and D. N. Seidman, "Simultaneous segregation at coherent and semicoherent heterophase interfaces." *Phys. Rev. Lett.*, **105**, 076102-1 (2010).
81. H. Zhou, W. Yao, C. Du, S. Song, and R. Wu, "Corrosion behavior of the Al₂Cu intermetallic compound and coupled Al₂Cu/Al." *Int. J. Electrochem. Sci.*, **12**, 9542 (2017).